Tracing CNO exposed layers in the Algol-type binary system u Her

V. Kolbas,[1] A. Dervişoğlu,[2] K. Pavlovski[1]* and J. Southworth[3]

[1]*Department of Physics, University of Zagreb, Bijenička cesta 32, 10000 Zagreb, Croatia*
[2]*Department of Astronomy & Space Sciences, Erciyes University, Kayseri, Turkey*
[3]*Astrophysics Group, Keele University, Staffordshire CV4 7AL, UK*

ABSTRACT

The chemical composition of stellar photospheres in mass-transferring binary systems is a precious diagnostic of the nucleosynthesis processes that occur deep within stars, and preserves information on the components' history. The binary system u Her belongs to a group of hot Algols with both components being B stars. We have isolated the individual spectra of the two components by the technique of spectral disentangling of a new series of 43 high-resolution échelle spectra. Augmenting these with an analysis of the *Hipparcos* photometry of the system yields revised stellar quantities for the components of u Her. For the primary component (the mass-gaining star), we find $M_A = 7.88 \pm 0.26\,M_\odot$, $R_A = 4.93 \pm 0.15\,R_\odot$ and $T_{eff,\,A} = 21\,600 \pm 220$ K. For the secondary (the mass-losing star) we find $M_B = 2.79 \pm 0.12\,M_\odot$, $R_B = 4.26 \pm 0.06\,R_\odot$ and $T_{eff,\,B} = 12\,600 \pm 550$ K. A non-local thermodynamic equilibrium analysis of the primary star's atmosphere reveals deviations in the abundances of nitrogen and carbon from the standard cosmic abundance pattern in accord with theoretical expectations for CNO nucleosynthesis processing. From a grid of calculated evolutionary models the best match to the observed properties of the stars in u Her enabled tracing the initial properties and history of this binary system. We confirm that it has evolved according to case A mass transfer. A detailed abundance analysis of the primary star gives C/N = 0.9, which supports the evolutionary calculations and indicates strong mixing in the early evolution of the secondary component, which was originally the more massive of the two. The composition of the secondary component would be a further important constraint on the initial properties of u Her system, but requires spectra of a higher signal-to-noise ratio.

Key words: binaries: eclipsing – binaries: spectroscopic – stars: fundamental parameters – stars: individual: u Her.

1 INTRODUCTION

The evolution of a star in a binary system is affected by the presence of its companion. Only a limited space is allowed for evolution due to the mutual gravitational pool of the components, and the star which was initially more massive will be the first to reach this limiting radius (i.e. the Roche lobe). At this point a rapid phase of mass transfer happens. Most of the more massive component is accreted by its companion, and an Algol-type binary system is formed. The previously more massive star is now a low-mass subgiant filling its Roche lobe, and its companion is now the hotter and more massive component with the characteristics of a main-sequence star. The mass-transfer scenario, first hypothesized by Crawford (1955), is a well-established solution to the Algol paradox (cf. Hilditch 2001).

This evolutionary process causes many observable effects (changes in orbital period, erratic light variability, distorted radial velocity, RV, curves, etc.), but one is particularly important. Up to 80 per cent of the mass of the initially more massive star can be lost, exposing layers which were originally deep within the star and have been altered by thermonuclear fusion during the star's main-sequence evolution. Some of the material transferred to the companion is similarly altered. The surface chemical compositions of both stars are therefore a precious diagnostic of the nucleosynthesis processes that occur deep within stars. The abundance pattern in Algol-type binaries could reveal their past, and would be strong evidence for postulated mass transfer between the components (cf. Sarna & De Greve 1996).

In pioneering studies, a general trend has been revealed with an underabundance of carbon and an overabundance of nitrogen relative to solar values (Parthasarathy, Lambert & Tomkin 1983; Cugier & Hardorp 1988; Cugier 1989; Tomkin, Lambert & Lemke 1993). This is in line with expectations for the CNO cycle, which is

*E-mail: pavlovski@phy.hr

dominant during the early evolution of a high-mass star (Przybilla et al. 2010). However, for Algol systems, this picture may be altered depending on the initial conditions, component masses and the mass ratio (Sarna 1992). If a deep convective layer has developed, a standard cosmic abundance pattern is expected instead (Sarna & de Greve 1994).

Early observational studies were hampered by line blending and/or the relative faintness of the secondary star. Therefore, a very limited line list was studied. The methods of spectral disentangling (SPD; Simon & Sturm 1994; Hadrava 1995) and Doppler tomography (Bagnuolo & Gies 1991), in conjunction with big advances in high-resolution spectrographs, now make possible separation of the individual spectra of the components. These disentangled spectra in turn make feasible a precise determination of the components' effective temperatures (T_{eff}s) and photospheric chemical abundances, as elaborated by Hensberge, Pavlovski & Verschueren (2000) and Pavlovski & Hensberge (2005).

As already stated, the photospheric abundance pattern in mass-transfer binary systems preserves information on their past history. The initial characteristics of these systems vary, and a fine spectroscopic analysis of the abundance patterns can provide additional evidence for proper discrimination between different evolutionary paths and mass-loss mechanisms (e.g. what fraction of mass-loss is by stellar wind, are mass-loss and angular momentum changes conservative or non-conservative, etc.). With this aim in mind, we initiated an observational project of high-resolution échelle spectroscopy of bright Algol-type (semidetached) binary systems.

The binary system u Her (68 Her, HD 156633) belongs to a small group of early-type semidetached systems first recognized by Eaton (1978). It differs from normal Algols in several aspects: (i) the total mass is larger; (ii) the components are more similar in T_{eff}; and (iii) the mass ratio is larger (Hilditch 1984). Their evolutionary paths might also differ from those of normal Algols, which are the product of case B mass transfer: it is supposed that in 'hot Algols' case A mass transfer is involved (Webbink 1976). This was supported by the theoretical calculations of Nelson & Eggleton (2001).

u Her is an eclipsing and double-lined spectroscopic binary with a rich observational history thanks to its brightness ($V = 4.80$ mag at maximum light). The most recent studies of u Her are those of Hilditch (2005) and Saad & Nouh (2011). Both studies contributed with new spectroscopic observations, but their measured stellar masses differ. Whilst the masses for the components in Saad & Nouh (2011) are similar to earlier determinations (cf. Kovachev & Seggewiss 1975; Hilditch 1984), Hilditch's (2005) revised values are considerably greater, by 2.0 ± 0.7 and 0.6 ± 0.3 M$_\odot$ for the primary (mass-gaining) and secondary (mass-losing) components, respectively.

The carbon abundance for the primary star has been estimated in two studies, which disagree. First, Cugier (1989) analysed UV spectra obtained with the *International Ultraviolet Explorer* (*IUE*) satellite for a group of Algols, and concluded that u Her shows an essentially cosmic abundance of carbon. Contrarily, an analysis of optical spectra by Tomkin et al. (1993) revealed a carbon deficiency in the primary star with respect to the average carbon abundance of single B-type standard stars.

The primary goal of our study is the determination of the photospheric chemical composition for the primary component in u Her. We have secured a new series of the high-resolution échelle spectra and used SPD to isolate the spectra of the two components. This enables us to determine the atmospheric parameters and the elemental abundances from the entire optical spectral range. As a by-product the two masses were also derived and compared to the previous

solutions. In Section 6, an overview of the evolutionary calculations is presented, and a possible evolutionary path for the components is discussed. The observed [N/C] abundance ratio strengthens our conclusions from the model calculations.

2 SPECTROSCOPY

We obtained 43 spectra of u Her in the course of two observing runs (2008 May and August) at the Centro Astronómico Hispano Alemán (CAHA) at Calar Alto, Spain. We used the 2.2 m telescope, FOCES échelle spectrograph (Pfeiffer et al. 1998), and a Loral #11i CCD binned 2×2 to decrease the readout time. With a grating angle of 2724, prism angle of 130 and a 150 μm slit we obtained a spectral coverage of roughly 3700–9200 Å in each exposure, at a resolving power of $R \approx 40\,000$. Wavelength calibration was performed using thorium–argon exposures, and flat-fields were obtained using a tungsten lamp. The observing conditions were generally good but several exposures suffered from the presence of thin clouds.

The échelle spectra were bias-subtracted, flat-fielded and extracted with the IRAF[1] échelle package routines. Normalization and merging of the orders was performed with great care, using custom programs, to ensure that these steps did not cause any systematic errors in the resulting spectra.

3 SPECTROSCOPIC ORBIT THROUGH SPECTRAL DISENTANGLING

In SPD the individual component spectra are isolated simultaneously with the determination of the optimal set of orbital elements. The reliability of the separated spectra and orbital elements depends on the spectral characteristics of the components and their contribution to the total light of the system.

According to previous photometric solutions for u Her (cf. Hilditch 2005), the primary star is about 3.3 times brighter than the secondary. Also, their T_{eff}s are quite different. For the primary star ($T_{eff} \sim 22\,000$ K), the He I lines are expected to be at maximum strength. For the secondary star ($T_{eff} \sim 12\,500$ K), the He I lines should be quite weak but the Balmer lines stronger than for the primary. Metal lines, quite prominent in the primary, are much weaker in the secondary, both intrinsically and due to the component's relative faintness. Therefore, we concentrate on the Balmer and helium lines, putting more emphasis on the latter.

The Fourier method (Hadrava 1995), is the best choice for disentangling spectra covering an extensive spectral range with high spectral resolution. The code FDBINARY[2] (Ilijić et al. 2004) was used to perform SPD in spectral regions centred on the prominent helium and Balmer lines, covering 50–150 Å in each region (Fig. 1). The orbital solution obtained by SPD yields velocity amplitudes of $K_1 = 94.6 \pm 2.3$ km s^{-1} and $K_2 = 267.4 \pm 3.3$ km s^{-1}, and thus a mass ratio of $q = 0.354 \pm 0.010$, under the assumption of a circular orbit.

In both recent studies of u Her, a spectroscopic orbit was determined by SPD, but the results are in astonishingly poor agreement for such a bright object. Our values for the two velocity amplitudes are much closer to those found by Saad & Nouh (2011) and in clear disagreement with those from Hilditch (2005). Saad & Nouh (2011) based their solution on red optical spectra covering Hα and the He I 6678 Å line, finding $K_1 = 98$ km s^{-1} and
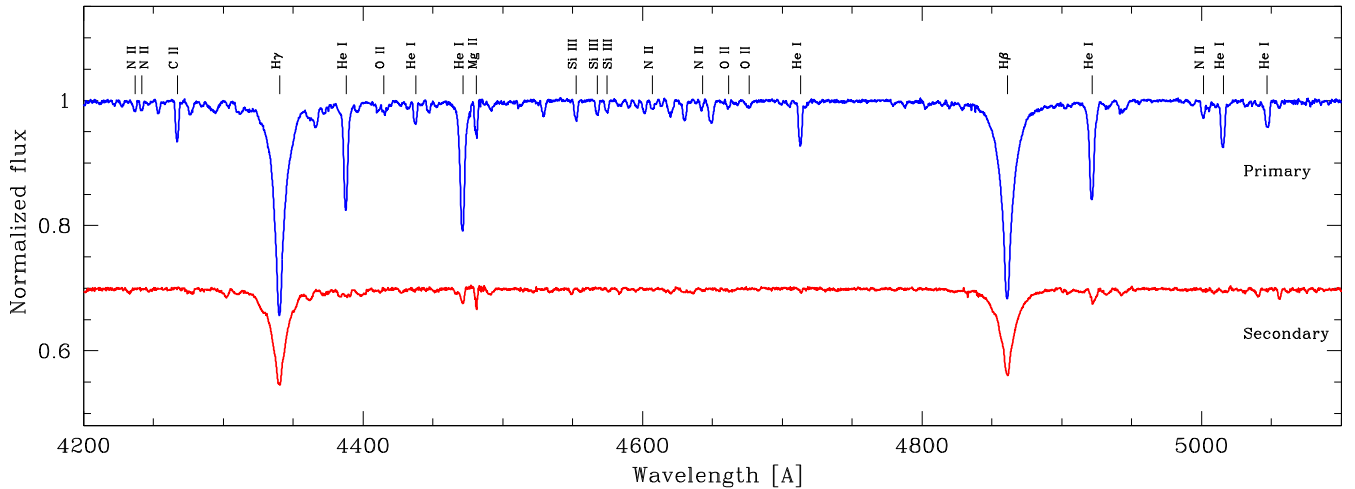
Figure 1. The portion of disentangled spectra of both components of the binary system u Her in the region of the Balmer lines Hγ and Hβ. The spectrum of the secondary component was shifted down by 0.3 for clarity. The lines of hydrogen, helium and some metals used in the analysis of the primary component are labelled.

$K_2 = 265 \, \text{km s}^{-1}$ (no errors are quoted). Hilditch (2005) used grating spectra covering 450 Å of the blue-optical spectral region, finding $K_1 = 102.4 \pm 2.4 \, \text{km s}^{-1}$ and $K_2 = 274.8 \pm 0.9 \, \text{km s}^{-1}$. In particular, K_2 is considerably higher than earlier measurements. We suspect that the disagreement between the orbital solutions stems primarily from the different spectral resolution employed; Hilditch's grating spectra have a resolution of 0.46 Å px^{-1}, while our échelle spectra have a much higher resolution of 0.02 Å px^{-1}. However, the study by Kovachev & Seggewiss (1975) yielded $K_1 = 95.6 \pm 1.4 \, \text{km s}^{-1}$ and $K_2 = 263 \pm 3 \, \text{km s}^{-1}$, from photographic spectra of a similar resolution to Hilditch's digital spectra, and RV measurements by the classical oscilloscopic method.

Discrepancies in the masses calculated from the above spectroscopic solutions are more pronounced for the primary, $M_1 = 7.9$ to $8.8 \, \text{M}_\odot$, than for the secondary, $M_2 = 2.8$ to $3.3 \, \text{M}_\odot$. In his final solution, Hilditch (2005) corrected the two velocity amplitudes for the distorted shape of the stars and their mutual irradiation, resulting in masses of $M_1 = 9.61 \pm 0.14 \, \text{M}_\odot$ and $M_2 = 3.48 \pm 0.13 \, \text{M}_\odot$. These are, as noted by Hilditch, considerably higher than in earlier solutions for u Her.

4 LIGHT-CURVE MODELLING

Since u Her is a bright object it has a long history of photometric measurements. All published ground-based light curves show night-to-night variations and a scatter of about 0.04 mag (Söderhjelm 1978; Rovithis & Rovithis-Livaniou 1980; van der Veen 1984). In contrast, the *Hipparcos* satellite photometry (H_p passband) covers about 1160 d between 1989 and 1993, and is of good quality (Fig. 2). Hilditch (2005) discussed possible explanations for the erratic night-to-night variations and concluded that they are intrinsic to the system. Since no periodicity could be determined he flagged it as a semiregular variable. He asserted that the time coverage of the *Hipparcos* photometry corresponds to a quiescent period of the system. Therefore, we decided to reanalyse only the H_p photometry.

In a period analysis of 10 semidetached Algol-type binaries, İbanoğlu et al. (2012) found u Her to be the system with the smallest period changes. We used their ephemeris[3] during our analysis;

---

[3] In table 6 of İbanoğlu et al. (2012) there is a typo, confusing u Her with U Her, a common mistake in the literature, see Hilditch (2005).
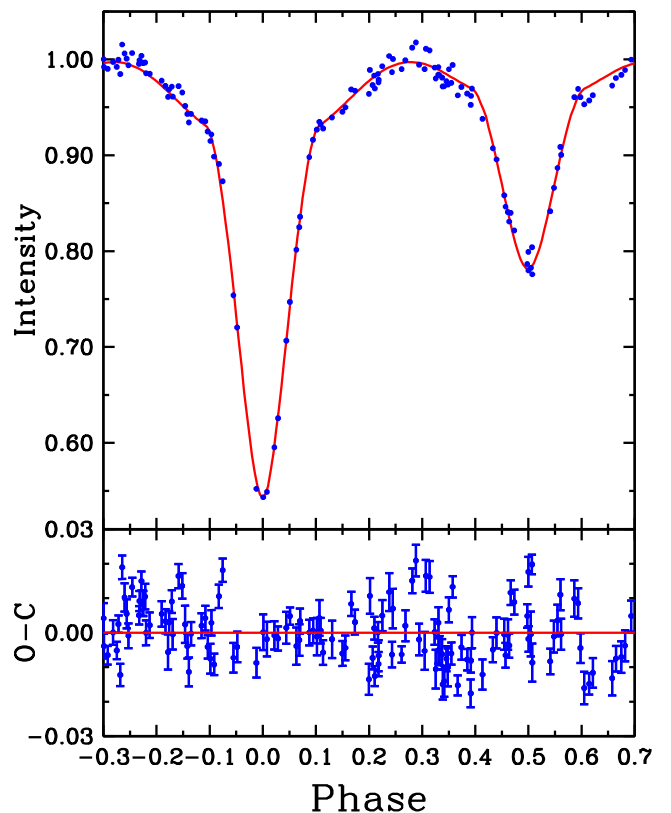
Figure 2. Observed phased *Hipparcos* H_p-band light curves of u Her with the best-fitting PHOEBE model light curves. The error bars are of similar size to the data points. In the lower panel, the residuals have been plotted to show the goodness of the fit.

$T_{\text{prim.min.}}(\text{HJD}) = 2447611.5007(15) + 2.05102685(68) \times E$ where the standard deviations in the last significant digits are given in brackets.

Initially, we set the primary's T_{eff} to 20 000 K, as derived by Hilditch (2005) using *uvby* photometry and the $[u - b] - T_{\text{eff}}$ calibration from Tomkin et al. (1993) and Napiwotzki, Schoenberner & Wenske (1993). In a second iteration, we fixed it at our

Table 1. Results from the solution of H_p band light curves of u Her.

Parameter	Unit	Value
Fixed parameters:		
Orbital period P	d	2.051 026 85
Primary eclipse time HJD	d	2 447 611.5007
Mass ratio q		0.354
T_{eff} of star A	K	21 600
Primary LD coefficients		0.434, 0.252
Secondary LD coefficients		0.568, 0.318
Gravity darkening		1.0, 1.0
Bolometric albedo		1.0, 1.0
Third light		0.0
Fitted parameters:		
Star A potential		3.437 ± 0.250
Orbital inclination	°	78.9 ± 0.4
T_{eff} of star B	K	$12\,700 \pm 140$
Derived parameters:		
$L_1/(L_1 + L_2)$		0.739 ± 0.026
Fractional radius of star A		0.330 ± 0.009
Fractional radius of star B		0.285 (fixed)

revised value of $T_{eff} = 21\,600 \pm 220$ K (Section 5.1). Our value for the primary T_{eff} agrees within 1σ with Hilditch's, who also noted that there is no significant effect on the light-curve solutions when values between 19 000 and 21 500 K are used.

In order to analyse the light curve we deployed the Wilson–Devinney (WD) code implemented into the PHOEBE package by Prša & Zwitter (2005). Our initial unconstrained system parameters immediately converged to a semidetached configuration. Thus, we used the MODE=5 option for subsequent solutions. Since WD uses Roche geometry, the solutions are sensitive to the mass ratio, which we fixed at the value derived from our orbital solution above, $q = 0.354 \pm 0.010$. Other fixed parameters in our light-curve calculations are listed in Table 1.

The orbital inclination, secondary-star T_{eff}, primary-star surface potential, phase shift, and fractional primary-star luminosity were put as adjustable parameters. We kept the other parameters as fixed. Iterations were carried out until convergence was achieved. The formal parameter uncertainties calculated by WD's differential correction solver are not trustworthy, so we implemented a more robust approach to error estimation. We simulated a range of solution sets around our fixed parameter values and calculated the χ^2 value of each. Then we accepted each parameter's 2σ confidence level as our error range, assuming that the χ^2 values follow a Gaussian distribution. In Table 1, we show the final parameter set and their corresponding error estimations. The computed light curve and residuals from observations is shown in Fig. 2.

5 SPECTRAL ANALYSIS OF BOTH COMPONENTS

5.1 The effective temperatures

To construct model atmospheres for the individual components of binary system, we first need to set their T_{eff}s and surface gravities ($\log g$s). When stars are in binary systems for which accurate masses and radii can be derived from RV and light curves, the resulting $\log g$ measurements have a much higher precision than those determinable from spectroscopic analysis alone. In the case of u Her, and even though our observational data give only a modest

accuracy in the masses and radii (about 3–4 per cent and 2–3 per cent, respectively) we measured $\log g$ values to about 0.013 dex for the primary and 0.018 dex for the secondary.

The availability of these $\log g$ measurements lifts the degeneracy between T_{eff} and $\log g$ as determined from Balmer line profiles. However, the trade-off is that the disentangled spectra of the components must be renormalized to their intrinsic continuum flux. Pure SPD returns the components' spectra relative to a common continuum level, and the individual spectra of the components are diluted by the factor proportional to their fractional contribution to the total light of the system. If no input spectra were obtained during eclipse (i.e. the component light ratio is the same for all spectra), the zeroth-order mode in the Fourier disentangling is singular, and an ambiguity in the proper renormalization of the disentangled spectra to their own continuum appears (Pavlovski & Hensberge 2005). Hence, external information on the light ratio is needed (see Pavlovski & Hensberge 2010; Pavlovski & Southworth 2012). In the case of u Her, we can use the light ratio as determined by the light-curve solution (Section 4), $l_1/l_2 = 0.300 \pm 0.003$, where l_1 and l_2 are the fractional contributions of the components to the total light of the system.

The optimal fitting of the Balmer lines in the renormalized component spectra to the grid of synthetic spectra was performed with our STARFIT code. This optimization routine uses a genetic algorithm inspired by the PIKAIA subroutine of Charbonneau (1995). The following parameters for each component can be either optimized or fixed: T_{eff}, $\log g$, light factor, projected rotational velocity ($v \sin i$), velocity shift, and continuum level adjustment. The velocity shift is needed because in SPD there is no absolute wavelength scale, and disentangled spectra are returned on a wavelength scale with an arbitrary zero-point. The reason for the continuum level adjustment is the fact that disentangled spectra are shifted according to the line blocking of the individual components, and an additive constant is needed to rectify disentangled spectra to a continuum of unity (Pavlovski & Hensberge 2005). This is the main improvement over our previous code GENFIT (Tamajo, Pavlovski & Southworth 2011). STARFIT can be run in constrained mode (simultaneous fit for both components with the condition that $l_1 + l_2 = 1.0$) or unconstrained mode (see Tamajo et al. 2011). For u Her, we ran STARFIT in unconstrained mode with the light ratio fixed to that from the light-curve model and the $\log g$ values of the stars fixed. Since the intrinsically broad Balmer lines are almost unaffected by the rotational kernel, the $v \sin i$ values for both components were first derived by iteratively fitting helium and metal lines. The T_{eff}s were then determined from the optimal fitting of the Hγ and Hβ lines. The results for T_{eff} and $v \sin i$ for both components are given in Table 2. The quality of the fits is illustrated in Fig. 3. The spectroscopically determined

Table 2. The absolute dimensions and related quantities determined for u Her. V_{synch} is the calculated synchronous rotational velocity.

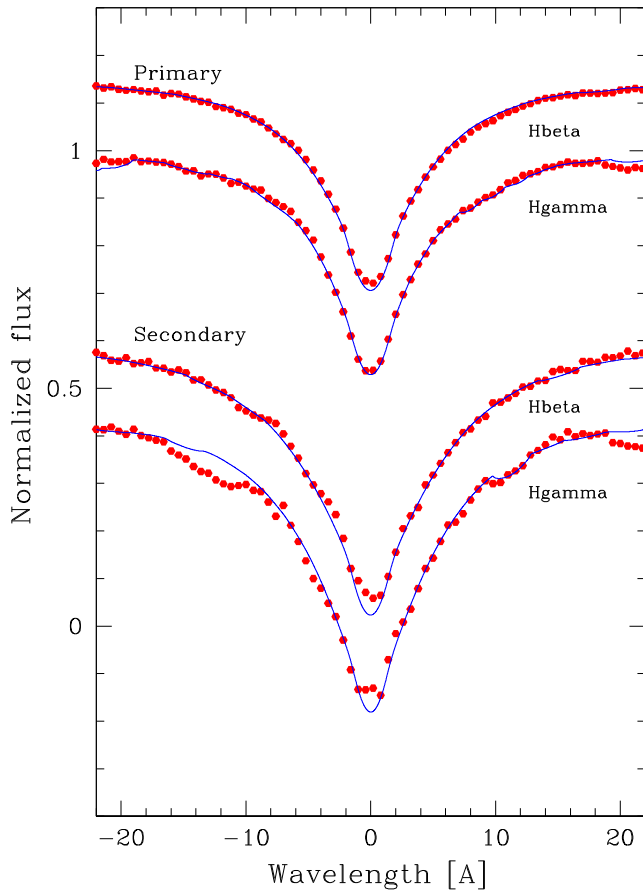| Parameter	Unit	Star A	Star B
Semimajor axis	$R_\odot$	14.95 ± 0.17	
Mass	$M_\odot$	7.88 ± 0.26	2.79 ± 0.12
Radius	$R_\odot$	4.93 ± 0.15	4.26 ± 0.06
$\log g$	cm s^{-2}	3.948 ± 0.024	3.625 ± 0.013
T_{eff}	K	$21\,600 \pm 220$	$12\,600 \pm 550$
$\log L$	$L_\odot$	3.68 ± 0.03	2.63 ± 0.08
$V_{eq} \sin i$	km s^{-1}	124.2 ± 1.8	107.0 ± 2.0
V_{synch}	km s^{-1}	121.7 ± 3.5	105.0 ± 1.5

Figure 3. The best-fitting synthetic spectra (lines) compared to the renormalized disentangled spectra (filled circles) of the two stars. For both components Hβ (upper) and Hγ (lower) profiles are shown.

$T_{\rm eff}$ for the secondary component is in perfect agreement with the results from the light-curve analysis (cf. Table 1).

5.2 Abundances

Theoretical spectra for the atmospheric parameters of the primary and varying microturbulence velocities ($v_{\rm turb}$) and elemental abundances were calculated in a 'hybrid' approach (Nieva & Przybilla 2007; Przybilla et al. 2010), which combines local thermodynamic equilibrium (LTE) atmospheres and non-local thermodynamic equilibrium (non-LTE) line-formation calculations. We computed model atmospheres with the ATLAS9 code, which assumes plane-parallel geometry, chemical homogeneity, and hydrostatic, radiative and LTE. Line blanketing was realized by means of opacity distribution functions. Solar abundances were adopted in all computations. Non-LTE level populations and model spectra were obtained with the DETAIL and SURFACE codes (Giddings 1981; Butler & Giddings 1985). Non-LTE level populations and synthetic spectra of H, He, C, N, O, Mg, Si and Al were computed using the most recent model atoms (see table 3 in Nieva & Przybilla 2012). The $v_{\rm turb}$ was determined from the condition of null correlation between O abundance and equivalent width. Oxygen is used for this purpose since the O lines are the most numerous in spectra for $T_{\rm eff}$s similar to that of the primary component. Only the lines selected by Simón-Díaz (2010) were used. The $v_{\rm turb}$ determined, 2 ± 1 km s^{-1}, is in the range of typical values for early B-type stars on the main sequence (cf. Simón-Díaz 2010; Nieva & Simón-Díaz 2011; Nieva & Przybilla 2012; Nieva 2013).

Table 3. Photospheric helium abundance for the primary component of u Her as derived from different He I spectral lines. The abundances are given as the fractional number of helium atoms to the total number of atoms in the stellar atmosphere (N(H) + N(He)).

Line	N(He)	Line	N(He)
4387.9	0.087 ± 0.008	5015.7	0.075 ± 0.006
4437.6	0.101 ± 0.010	5047.7	0.091 ± 0.007
4471.5	0.088 ± 0.007	5876.7	0.095 ± 0.002
4713.2	0.078 ± 0.006	6678.1	0.086 ± 0.007
4921.9	0.104 ± 0.005		

Table 4. Estimated photospheric abundances for different ions in the atmosphere of the primary component of u Her. Abundances are expressed relative to the abundance of hydrogen, $\log \epsilon$(H) = 12.0.

Line	$\log \epsilon$(X)	Line	$\log \epsilon$(X)	Line	$\log \epsilon$(X)
C II		O II		Mg II	
4267.00	7.90	4185.46	8.55	4481.13	7.50
5132.95	7.95	4189.79	8.70	5264.22	7.40
5137.26	7.97	4414.88	8.55	5401.54	7.50
5143.40	7.95	4416.97	8.62	Si II	
5151.08	7.85	4590.97	8.70	4128.05	7.55
N II		4596.20	8.68	4130.88	7.40
4227.75	8.00	4609.42	8.50	Si III	
4236.91	7.98	4661.63	8.62	4552.62	7.48
4241.80	7.95	4673.75	8.65	4567.82	7.37
4447.03	8.00	4676.23	8.65	4574.76	7.55
4507.56	8.00	4677.07	8.70	4716.65	7.70
4607.15	8.05	4698.48	8.60	4819.72	7.50
4613.86	8.00	4699.21	8.68	4828.96	7.35
4643.09	7.90	4703.18	8.48	Al III	
4803.27	8.05	4705.35	8.55	4149.92	6.30
4987.38	8.00	5206.64	8.50	4479.97	6.40
4994.36	8.02			4512.54	6.20
5001.47	7.95			4528.94	6.40
5007.31	7.83				
5010.62	7.90				
5045.09	7.93				
5495.65	8.03				
5666.63	7.85				

Abundances are estimated by line profile fitting and are listed for all transitions calculated and for lines which are not severely blended. They are given in Table 3 for He I and Table 4 for all other ions. The mean values of abundances and their uncertainties for all elements studied in the disentangled spectrum of the primary component are given in Table 5. The uncertainties in the abundances are calculated from the scatter in the estimated abundances for different lines, and for 1σ deviations in the $T_{\rm eff}$ and $v_{\rm turb}$. However, the prevailing uncertainty in abundances comes from the scatter between different lines.

Cugier (1989) determined the carbon abundances in the mass-gaining components of six Algol-type systems, including u Her. He used UV spectra taken with the *IUE*, and measured the total equivalent widths of the C II multiplets at 1334.5–1335.7 Å and 1323.8–1324.0 Å. He constrained the components' $T_{\rm eff}$s from the UV flux distribution and van der Veen's (1984) photometric solution, finding $T_{\rm eff, 1} = 22\,200 \pm 1500$ K and $T_{\rm eff, 2} = 13\,300 \pm 1000$ K. After correction for non-LTE effects he found $\log \epsilon$(C) = 8.62 ± 0.30, and concluded that the primary of u Her shows no indication of a

Table 5. Photospheric abundances derived for the primary component of u Her. Abundances are expressed relative to the abundance of hydrogen, $\log \epsilon (H) = 12.0$. The third column gives the number of lines used. Present-day cosmic abundances from Galactic OB stars (Nieva & Przybilla 2012) are given in the fourth column, and the fifth column lists the solar abundances from Asplund et al. (2009).

El.	$\log \epsilon (X)$	N	[X/H]	OB stars	Sun
He	10.99 ± 0.05	6	0.02 ± 0.05	10.99 ± 0.01	10.97 ± 0.01
C	7.92 ± 0.02	5	-0.47 ± 0.05	8.33 ± 0.04	8.39 ± 0.05
N	7.97 ± 0.02	17	0.20 ± 0.06	7.79 ± 0.04	7.78 ± 0.06
O	8.61 ± 0.02	16	-0.05 ± 0.05	8.76 ± 0.05	8.66 ± 0.05
Mg	7.47 ± 0.03	3	-0.06 ± 0.09	7.56 ± 0.05	7.53 ± 0.09
Si	7.49 ± 0.04	8	-0.02 ± 0.06	7.50 ± 0.05	7.51 ± 0.04
Al	6.32 ± 0.05	4	-0.05 ± 0.06		6.37 ± 0.04

change in the carbon abundance, in contrast to other Algols in his sample.

Tomkin et al. (1993) reported high-resolution CCD spectra of the C II 4267 Å line in the same Algol systems that were studied by Cugier (1989) and Cugier & Hardorp (1988). They estimated carbon abundances in the Algol primaries differentially with respect to single B-type stars. They derived the T_{eff}s from Strömgren photometry using the calibration by Napiwotzki et al. (1993), finding $T_{1,\,\text{eff}} = 20\,000$ K. Tomkin et al. obtained a carbon abundance of [C/H] $= -0.34$ with respect to the average abundance of the standard stars, $\log \epsilon (C) = 8.28$.

The carbon abundance determined in this work, $\log \epsilon (C) = 7.92 \pm 0.02$, is based on the measurements of five lines, and is in almost perfect agreement with the value derived by Tomkin et al. (1993) from a single carbon line. A considerable difference in the adopted T_{eff}s between Tomkin el al. and our values has little influence probably because the temperature dependence of the carbon line strengths is weak in the region from 19 000 to 24 000 K, where C II lines reach their maximum strength. A comparison between the renormalized disentangled spectrum of the primary component and a grid of the theoretical spectra for several C II lines in the 5130–5154 Å region is shown in Fig. 4 (upper panel).

The nitrogen abundance is based on measurements of 17 lines, and is firmly determined to be 0.20 ± 0.06 dex above the solar value. In turn, this gives the [N/C] abundance ratio 0.05 ± 0.03 dex, considerably different to the 'standard' cosmic (-0.54 ± 0.06; Nieva & Przybilla 2012) or solar (-0.61 ± 0.08; Asplund et al. 2009) values. Changes in the N/C abundance ratio in the course of mass transfer preserve the imprint of the components' evolutionary history. These findings are discussed in the next section, in the context of the chemical evolution in mass-transfer binary systems, and provide a strong argument for case A evolution for the u Her binary system. In Fig. 4 (middle panel), the comparison of the three N II lines in the 4225–4245 Å spectral region to a grid of theoretical spectra is shown. Fig. 4 (bottom panel) shows a portion of the spectrum containing O II lines.

Helium is a final product of CNO nucleosynthesis and its abundance steadily increases during the components' evolution. The helium abundance derived for the primary component is in perfect agreement with the value found by Nieva & Przybilla (2012) for OB stars, albeit that the uncertainty in our determination is quite large. The quality of the fits for selected He I lines is shown in Fig. 5. The model calculations (Section 6) show an increase in the helium abundance by mass fraction after the phase of mass transfer by a factor of approximately 1.25, which settled again to almost the initial value after thermohaline mixing. The remaining helium enhancement of
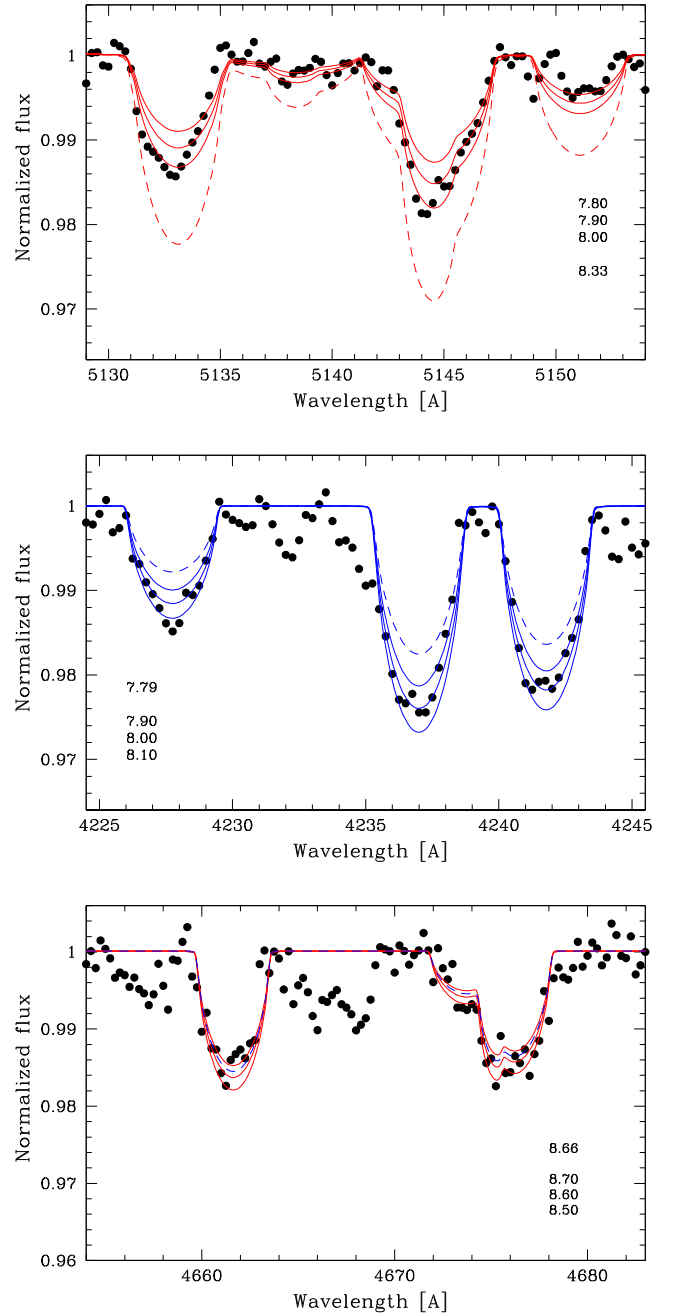

Figure 4. Comparison between the renormalized disentangled spectrum of the primary component in u Her (filled circles) and a grid of theoretical spectra computed assuming different abundances. From top to bottom, the panels show selected lines for carbon, nitrogen, and oxygen, respectively. The abundances used for the theoretical spectra are indicated in the labels. Spectra calculated for the 'present-day cosmic abundances' for the Galactic OB stars (Nieva & Przybilla 2012) are indicated by dashed lines.

only 2 per cent could not be detected in our measurements because it is below the level of the uncertainties.

The three metals magnesium, silicon and aluminium have a marginally subsolar abundance, giving on average [M/H] $= -0.04 \pm 0.03$. In our subsequent modelling, we therefore assumed a solar composition.

Despite the importance, we did not attempt a detailed abundance analysis for the secondary star because its renormalized
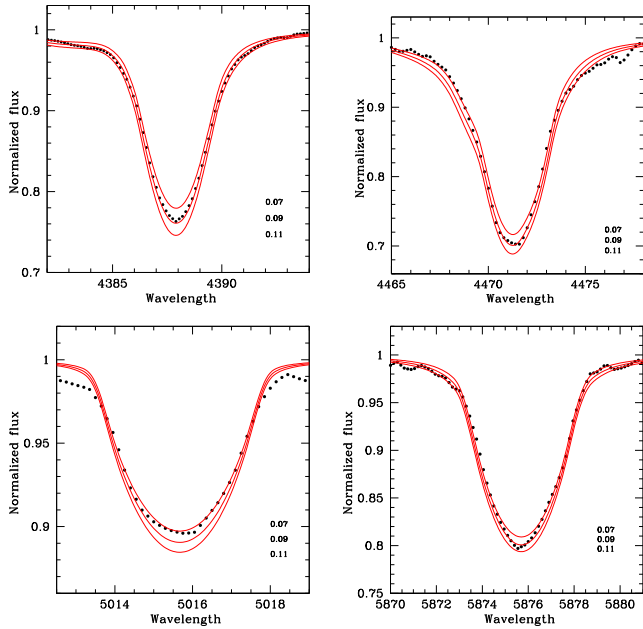
Figure 5. The quality of the fits for selected He I lines at 4387.9, 4471.5, 5015.7 and 5876.7 Å to the theoretical spectra (lines). Theoretical spectra were calculated for the stellar parameters listed in Table 2; the assumed helium abundances are indicated in the bottom-right corner of each panel, and are expressed by a fraction of the helium atoms to the total number of atoms in the stellar atmosphere. The renormalized disentangled spectra are represented by filled circles.

disentangled spectrum suffers from low signal-to-noise ratio (S/N). In combination with a high projected rotational velocity, $v \sin i \sim 100 \text{ km s}^{-1}$, this makes the results unreliable. However, we notice a complete absence of the C II 4267 Å line, which should be visible given the T_{eff} of this star. This is illustrated in Fig. 6 in which C II 4267 Å lines for both components are shown. The optimal fit for the primary's line gives the abundance $\log \epsilon(C) = 7.90$ (cf. Table 5). It is clear that the primary's carbon abundance does not hold for the secondary. A rough estimate yields a carbon abundance for the secondary of $\log \epsilon(C) \leq 7.5$, which is more than an order of magnitude lower than the 'present-day cosmic abundance' of carbon (Nieva & Przybilla 2012), also indicated in Fig. 6. The calculations to be presented in Section 6 give a depletion of carbon by a factor of ~ 7.5 after mass transfer phase has been settled, hence the expected carbon abundance in the atmosphere of the secondary would be $\log \epsilon(C) \sim 7.4$. Non-detection of the secondary's C II 4267 Å line therefore corroborates the predictions of the theoretical models. However, additional spectra of u Her are needed to enhance the S/N of disentangled spectrum of the secondary star to enable a more definitive conclusion.

6 EVOLUTIONARY ANALYSES

As discussed above, u Her belongs to a special group of hot Algols, which differ from ordinary systems by having a larger total mass and mass ratio. 80 years of accumulated photometric data show no evidence for an orbital period change, which suggests that u Her is in a very advanced episode of slow mass transfer (SMT). But this finding is puzzling given its short orbital period, as one would expect a wider orbit at the end of the mass transfer phase. In any binary, whenever mass transfer occurs from the higher mass to the lower mass companion, it is expected that the orbital period decreases
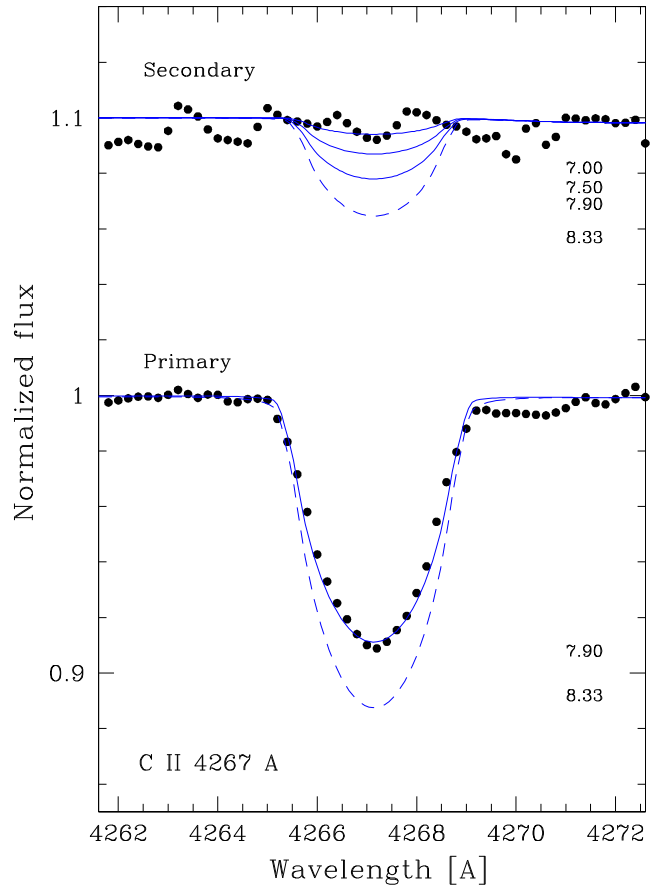

Figure 6. Renormalized line profiles of C II 4267 Å for the components of u Her. The secondary spectrum is shifted by +0.1 for clarity. Theoretical spectra calculated for different abundances (indicated in the labels) are shown for comparison. Dashed lines represent the 'present-day cosmic abundance' of carbon derived by Nieva & Przybilla (2012). Whilst the carbon abundance is depleted in the primary, it is almost an order of magnitude less in the atmosphere of the secondary component. See Section 5.2 for details.

until mass ratio reversal. So, tracing back the mass exchange clearly shows that this system may be in a contact configuration during the rapid mass transfer (RMT) phase.

It has been considered that u Her is a product of case A mass transfer (Webbink 1976). The first detailed binary evolution models have been done by Nelson & Eggleton (2001). Based on a grid of 5500 binary tracks with various values of initial primary mass, mass ratio and period, they found that the best-fitting initial model to produce a system like u Her has an initial donor-star mass of $M_{\text{d}}^{\text{i}} \sim 6.31 \text{ M}_\odot$, a mass ratio of $q^{\text{i}} \sim 1.41$ and an orbital period of $P^{\text{i}} \sim 1.32$ d. But they restricted their calculations to a conservative approach and avoided all contact encounters during mass transfer. Their result for u Her can therefore be taken as a maximum initial mass and period pair which cannot get into contact during the RMT phase.

de Mink, Pols & Hilditch (2007) extended this study with 20 000 detailed calculations of binary evolutionary tracks using a modified code based on that of Nelson & Eggleton (2001). They modified the Nelson and Eggleton code so that stellar structure equations of both stars are solved simultaneously, which is needed for accurately modelling mass transfer phases. Moreover, they accounted for non-conservative mass-loss and short contact phases during RMT, and concentrated on binaries in the Small Magellanic Cloud.

de Mink et al. (2007) suggested a new subtype of Algol systems [AR (rapid contact) → AN (no contact)] which shows a short-lived contact phase during the thermal response of the mass gainer to the RMT. After this the mass gainer restores its thermal equilibrium and shrinks, then mass transfer proceeds. To evaluate non-conservative evolution, they introduced a mass transfer efficiency parameter (β) which is a measure of how much matter is lost relative to that transferred. For the angular momentum evolution, they assumed that all the matter is lost via bi-polar emission from the mass-accreting star hence carries this star's specific angular momentum. One of the hot Algols in their sample (OGLE 09 064498) has a configuration very close to that of u Her: $M_p \sim 8.4 \pm 0.7\,M_\odot$, $q \sim 0.323$ and $P \sim 2.64$ d. The best-fitting initial model that they found had $M_d^i \sim 7.10\,M_\odot$, $q^i \sim 1.68$ and $P^i \sim 1.34$ d.

Instead of making a large grid of binary tracks which is more suited for a large sample of systems, we specifically prepared initial models for u Her for different initial mass ratios and mass-loss rates. Since the uncertainty on angular momentum loss has a big influence on our understanding of binary evolution, there is little value in using a very fine grid in parameter space. We then made some simplifications to reduce the number of initial models to reach plausible results. After determining the initial parameters, we searched for the best-fitting models produced by the binary evolution code in this grid.

We first considered four main sets of initial mass ratios q^i: 1.25, 1.50, 1.75 and 2.00. These are typical values to produce Algol-like systems at the end of mass transfer. We did not go beyond $q^i > 2.0$ because mass-gaining stars in these systems are unlikely to regain thermal equilibrium during RMT. To prepare a subset of initial models to take into account non-conservative mass transfer, we adopted the approach of de Mink et al. (2007). The mass transfer efficiency parameter β is defined as

$$\beta = 1 - \left| \frac{\dot{M}_g}{\dot{M}_d} \right| \qquad 0 \le \beta \le 1, \tag{1}$$

where g denotes the mass gainer and d the mass donor. From equation (1), one can easily see that $\beta = 0$ corresponds to conservative evolution. To evaluate angular momentum loss, we used the Hurley, Tout & Pols (2002) approximation which assumes that mass-loss takes the specific angular momentum of the mass-losing star. This is likely true for case A evolution due to the lack of an accretion disc producing bipolar mass-loss. Using this approximation and taking logarithmic differentiation of the angular momentum equation for a two-mass system

$$J^2 = \left(G \frac{M_d^2 M_g^2}{M_d + M_g} \right) 4\pi^2 A, \tag{2}$$

where A is a separation of binary, one can easily derive a relation for the orbital period evolution with the help of Kepler's second law:

$$\frac{P^f}{P^i} = \left(\frac{M_d^i + M_g^i}{M_d^f + M_g^f} \right)^{1/2} \left(\frac{M_g^i}{M_g^i + (1-\beta)(M_d^i - M_d^f)} \right)^3$$
$$\times \left(\frac{M_g^i + M_d^i}{M_g^i + (1-\beta)M_d^i + \beta M_d^f} \right)^{-3/2} \left(\frac{M_d^i}{M_d^f} \right)^{3(1-\beta)} \tag{3}$$

where superscripts i and f stand for initial and final parameters. The evolution of the total mass of system is adapted from Giuricin & Mardirossian (1981):

$$\frac{M_t^i}{M_t^f} = \frac{(1+q^i)\,[1+q^f(1-\beta)]}{(1+q^f)\,[1+q^i(1-\beta)]}. \tag{4}$$

Using a range of $\beta = [0.0, 0.10, 0.25, 0.50, 0.75]$, i.e. from conservative to highly non-conservative, we created 20 different initial models as candidate progenitors of u Her ($M_g^f \sim 7.9 \pm 0.26$, $q^f \sim 0.35 \pm 0.02$ and $P^f = 2.05$ d). But since equations (3) and (4) do not consider the properties of the stellar structure under the effect of mass transfer, one has to run detailed evolution codes to compare all of the observed properties of each companion as well as the orbit.

To calculate detailed binary evolution tracks, we used the Cambridge version of the STARS[4] code which was originally developed by Eggleton (1971, 1972). The most recent updates allow calculation of the evolution of each component simultaneously, the prescription of mass transfer and various physical improvements, and are explained in Stancliffe & Eldridge (2009). Since both observed and candidate initial masses of the components are in the intermediate-mass regime, we fixed the overshooting parameter at $\delta_{os} = 0.12$. We also assumed a solar composition in all of our components at the zero-age main sequence. Each binary evolution track was terminated whenever the mass gainer filled its Roche lobe at the end of SMT, i.e. reverse mass transfer.

In Table 6, we list the grid of our binary tracks. We show the initial parameters of the systems as well as the best-fitting model compared to the observed absolute parameters in Table 2. We checked each system's initial period with limiting period, i.e. the smallest period for given binary, via this equation from Nelson & Eggleton (2001):

$$P_{lim} \approx \frac{0.19 M_d^i + 0.47 M_d^{i\,2.33}}{1 + 1.18 M_d^{i\,2}}. \tag{5}$$

We also show the binary tracks and observed parameters of the system on the HR diagram in Fig. 7. Providing that each system starts with different initial parameters, the thermal responses of each component determine the length of the RMT and SMT phase. Most of the systems in Table 6 cannot accrete enough mass to reach the observed masses of the components of u Her before reverse mass transfer. Based on χ^2 minimization and visual inspection, the best-fitting model belongs to a group of conservative and high initial mass ratio systems. This was also the case for OGLE 09 064498 as discussed above. We also noticed a short-term contact phase, as also discussed by de Mink et al. (2007), in high initial mass ratio systems for the case of highly efficient mass transfer $q^i \ge 1.75$ and $\beta \le 0.25$.

Finding the best initial model parameters allowed us to trace the chemical evolution of both components during mass transfer. In Fig. 8a,b, we show the change in internal profile of the ratio C/N from the centre to the surface of each component. Due to the very different time-scales of the RMT and SMT phases, we plot this change versus the mass ratio instead of time. One can easily recognize the abrupt internal change in the mass gainer's profile which corresponds to the transition from RMT to SMT. From Fig. 8a, we find that the mass donor lost its mass up to the depth at which the CNO cycle reduced the C/N ratio from the cosmic (~ 3.2) to the equilibrium (~ 0.1) value. This nucleosynthetically processed material was then accreted on the surface of mass gainer. The accreted material had a higher mean molecular weight than that from the surface of the mass gainer. In such a case, one may expect thermohaline convection to mix this material and alter the surface composition. As shown by Stancliffe & Eldridge (2009), the effect of thermohaline mixing on the surface is negligible during RMT. We therefore ran all of our tracks without thermohaline mixing to

[4] Freely available at http://www.ast.cam.ac.uk/~stars/

Table 6. The list of initial and final parameters for our binary evolution grid. The first eight columns are input parameters of STARS evolution code runs. The remainder are the best-fitting model results for representing the current state of u Her. Run ID(1) is chosen to be the best-fitting progenitor system.

ID	q^i	β	M_t^i $M_\odot$	M_g^i $M_\odot$	M_d^i $M_\odot$	P_{lim} d	P^i d	M_d^f $M_\odot$	M_g^f $M_\odot$	P^f d	$\log L_d$ $L_\odot$	$\log T_d$ K	$\log R_d$ $R_\odot$	$\log L_g$ $L_\odot$	$\log T_g$ K	$\log R_g$ $R_\odot$
1	2.00	0.00	10.74	3.58	7.16	0.77	1.35	2.90	7.84	1.93	2.56	4.09	0.63	3.73	4.28	0.83
2	2.00	0.10	11.21	3.74	7.47	0.78	1.29	3.06	7.71	1.77	2.60	4.11	0.62	3.69	4.28	0.80
3	2.00	0.25	12.04	4.01	8.03	0.80	1.20	3.37	7.51	1.59	2.68	4.13	0.60	3.62	4.29	0.76
4	2.00	0.50	14.00	4.67	9.33	0.84	1.06	3.86	7.41	1.54	2.85	4.17	0.61	3.58	4.29	0.74
5	2.00	0.75	17.26	5.75	11.51	0.90	0.91	3.16	7.83	2.34	2.84	4.12	0.70	3.83	4.28	0.88
6	1.75	0.00	10.74	3.91	6.83	0.76	1.19	3.16	7.58	1.65	2.51	4.09	0.60	3.64	4.28	0.77
7	1.75	0.10	11.17	4.06	7.11	0.77	1.15	3.31	7.48	1.55	2.56	4.11	0.59	3.60	4.29	0.75
8	1.75	0.25	11.94	4.34	7.60	0.79	1.10	3.56	7.37	1.48	2.64	4.13	0.59	3.56	4.29	0.73
9	1.75	0.50	13.69	4.98	8.71	0.82	1.00	4.03	7.34	1.45	2.81	4.16	0.60	3.54	4.29	0.72
10	1.75	0.75	16.51	6.01	10.51	0.87	0.90	3.85	7.67	1.89	2.94	4.16	0.67	3.68	4.28	0.81
11	1.50	0.00	10.74	4.30	6.44	0.75	1.07	3.46	7.28	1.42	2.51	4.10	0.57	3.53	4.29	0.72
12	1.50	0.10	11.13	4.45	6.68	0.76	1.05	3.57	7.25	1.39	2.56	4.12	0.57	3.52	4.29	0.71
13	1.50	0.25	11.81	4.72	7.09	0.77	1.01	3.80	7.19	1.35	2.64	4.14	0.57	3.49	4.29	0.70
14	1.50	0.50	13.34	5.33	8.00	0.80	0.96	4.02	7.32	1.44	2.77	4.15	0.60	3.53	4.29	0.72
15	1.50	0.75	15.70	6.28	9.42	0.84	0.91	4.12	7.60	1.71	2.93	4.17	0.65	3.63	4.28	0.77
16	1.25	0.00	10.74	4.77	5.97	0.73	0.98	3.82	6.92	1.22	2.57	4.13	0.54	3.41	4.28	0.66
17	1.25	0.10	11.07	4.92	6.15	0.74	0.97	3.93	6.92	1.22	2.61	4.14	0.55	3.41	4.28	0.66
18	1.25	0.25	11.66	5.18	6.48	0.75	0.96	4.05	7.00	1.25	2.66	4.15	0.56	3.43	4.29	0.67
19	1.25	0.50	12.93	5.74	7.18	0.77	0.95	4.18	7.24	1.36	2.77	4.16	0.59	3.50	4.29	0.70
20	1.25	0.75	14.80	6.58	8.22	0.81	0.95	4.31	7.56	1.58	2.91	4.17	0.64	3.60	4.29	0.75

find the lower limit of the C/N ratio on the surface. We then applied thermohaline mixing to the model of the mass gainer to trace the change of chemical composition on its surface. As the thermohaline condition is not satisfied, we ignored the mass donor.

In Fig. 8c, we show the effect of thermohaline mixing on the whole internal profile of the star. Due to the material originating from different layers of mass donor, the outer layers of the stars have a variable composition profile. We find that the thermohaline mixing alters the surface composition of the stars on relatively short time-scale ($\sim10^5$ yr). Thus, we expect the surface C/N ratio of the gainer to be between non-mixed (~0.1) to mixed (~1). This result is in good agreement with our observed ratio of C/N $=0.89$.

We believe that determining the composition of the mass donor would be an important opportunity to constrain the initial evolutionary parameters. Such a situation would allow us to build a fine grid of binary tracks to compare results with observations as well as our understanding of the processes involved in binary evolution such as mass-loss mechanisms and thermohaline mixing. Even though we could not determine the surface composition of the mass donor, the lack of a prominent C II 4267 Å line compared to single stars of the same T_{eff} is a strong indication of decreased carbon abundance on the surface as a result of case A mass transfer. This is because, in a wider orbit, the mass donor may only lose the upper layers without reaching CNO processed regions. So far, our evolutionary calculation shows that u Her could start its evolution with $M_d^i \sim 7.16\,M_\odot$, $q^i \sim 2.00$ and $P^i \sim 1.35$ d.

7 CONCLUSIONS

Large-scale mass transfer in Algol-type binary systems not only leads to mass reversal and an exchange of the role between the components but also affects the photospheric chemical composition (Sarna 1992). Formerly deep layers can become exposed after a short-lived mass exchange. Therefore, tracing the photospheric elemental abundances of the components might help to constrain their past. Already in the first observational studies of this effect, a clear

evidence for carbon underabundance in the (brighter) primaries of Algol-type systems was found (Parthasarathy et al. 1983; Cugier & Hardorp 1988; Cugier 1989; Tomkin et al. 1993). More recent studies have not challenged that general conclusion (Glazunova, Mkrtichian & Rostophchin 2011; İbanoğlu et al. 2012).

The technique of SPD has opened up new possibilities in detailed spectroscopic studies of the stars in binary or multiple systems (cf. Pavlovski & Hensberge 2005; Pavlovski & Southworth 2009) since it enables isolation of the individual spectra of the components while simultaneously solving for the orbital elements. This allows a detailed determination of the photospheric chemical composition to be put on to much firmer ground.

This work addresses the chemical evolution of u Her, a hot Algol-type binary system. In hot Algols both components are of spectral type B, and hence more massive than in a typical Algol system. Consequently, the CNO cycle is more efficient and a greater alteration of the chemical composition is expected. A new set of 43 high-resolution échelle spectra were secured and analysed using SPD. Our conclusions are as follows.

(i) The masses and radii of the components are $M_A = 7.88 \pm 0.26\,M_\odot$ and $R_A = 4.93 \pm 0.15\,R_\odot$ for the primary (mass-gaining) star, and $M_B = 2.79 \pm 0.12\,M_\odot$ and $R_B = 4.26 \pm 0.06\,R_\odot$ for the secondary (mass-losing) star.

(ii) The T_{eff}s were determined from an optimal fitting of the Hγ and Hβ lines in the stars' disentangled and renormalized spectra. The light ratio was determined from re-analysis of the *Hipparcos* photometry. We find $T_{eff,\,1} = 21\,600 \pm 220$ K and $T_{eff,\,2} = 12\,600 \pm 550$ K.

(iii) The primary star's photospheric elemental abundances were derived from an extensive line list in the whole optical spectrum and exhibit a carbon depletion of [C/H] $= -0.47 \pm 0.05$ and a nitrogen enhancement of [N/H] $= 0.20 \pm 0.06$ with respect to the standard cosmic abundance pattern (Nieva & Przybilla 2012). The uncertainty in the helium abundance does not allow a firm
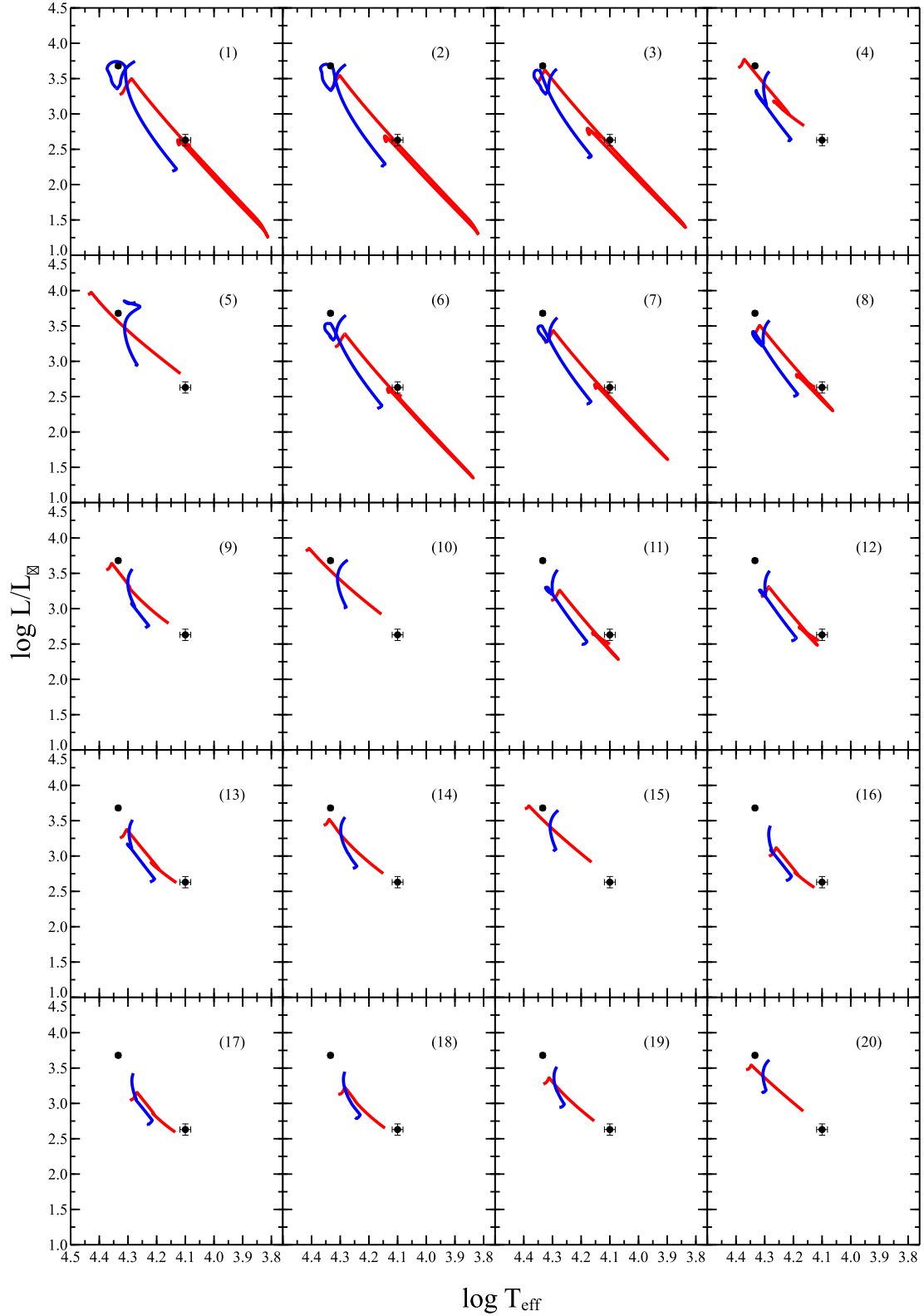
Figure 7. The grid of binary evolution tracks on the HR diagram. For given ID from Table 6, we show the evolution of the mass donor (red) and mass gainer (blue), as well as u Her's observed $\log L/L_\odot - \log (T_{eff}/K)$. Each set of tracks was terminated when the mass gainer fills its Roche lobe at the end of SMT.
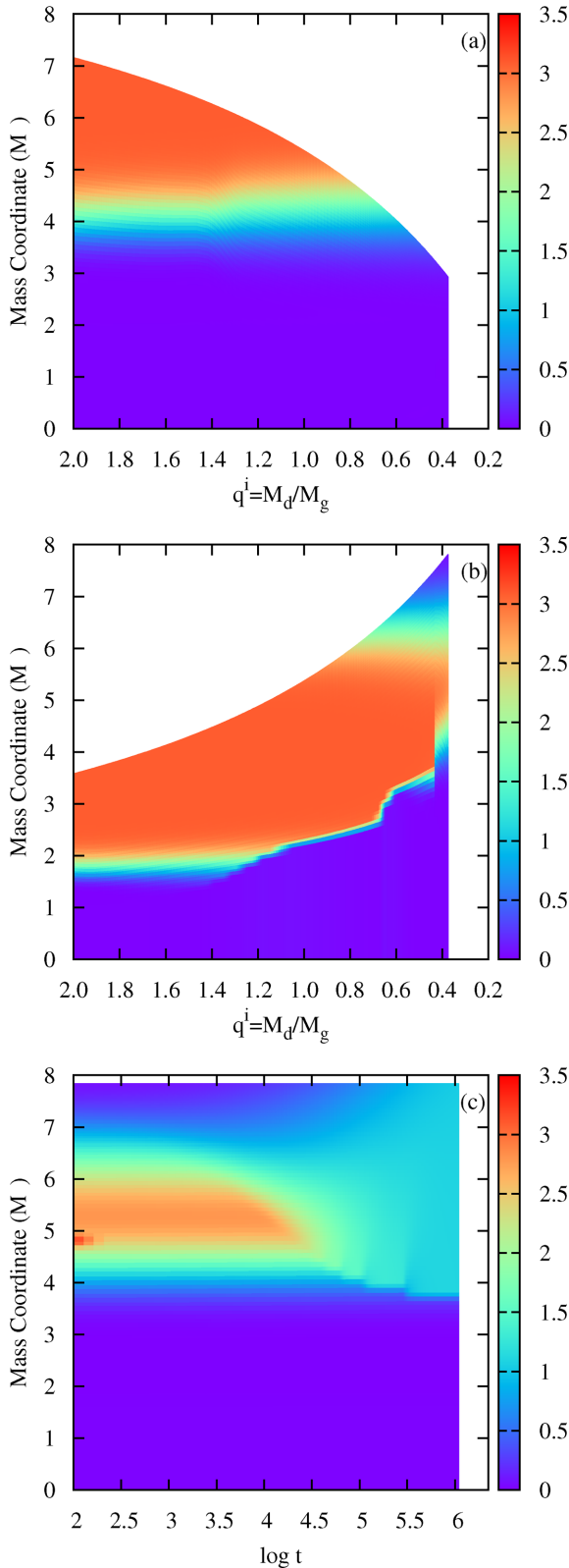
Figure 8. The internal C/N ratio changes at mass coordinates for the mass donor (panel 1) and the mass gainer (panel 2) during the mass ratio change as an indicator of RMT, derived from the evolution tracks of the best-fitting model – ID(1). The effect of thermohaline convection on the internal profile of mass gainer after SMT, $t = 0$ and $q^i < 0.4$ is shown in panel 3.

conclusion on the possible enhancement of the helium abundance ([He/H] $=0.02 \pm 0.05$).

(iv) Theoretical evolutionary calculations reproduce the current characteristics of the system from a progenitor binary with initial masses $M_d \sim 7.2\,M_\odot$ and $M_g \sim 3.6\,M_\odot$, and an initial period $P_i \sim 1.35$ d. The calculations have shown that thermohaline mixing alters the surface composition of stars on a relatively short time-scale, $t \sim 10^5$ yr. The observed C/N abundance ratio ($\sim$0.9) corroborates this picture and indicates a strong mixing of the stellar material.

(v) The composition of the secondary component would be a further important constraint on the initial properties of the u Her system, but requires spectra of a higher S/N. A non-detection of the C II 4267 Å line corroborates the model calculations and a general picture emerged from the study of the primary's photospheric chemical composition.

ACKNOWLEDGEMENTS

REFERENCES

Asplund M., Grevesse N., Sauval A. J., Scott P., 2009, ARA&A, 47, 481
Bagnuolo W. G., Gies D. R., 1991, ApJ, 376, 266
Butler K., Giddings J. R., 1985, Newsl. Anal. Astron. Spectra, 9
Charbonneau P., 1995, ApJS, 101, 309
Crawford J. A., 1955, ApJ, 121, 71
Cugier H., 1989, A&A, 214, 168
Cugier H., Hardorp I., 1988, A&A, 202, 101
de Mink S. E., Pols O. R., Hilditch R. W., 2007, A&A, 467, 1181
Eaton J. A., 1978, Acta Astron., 28, 601
Eggleton P. P., 1971, MNRAS, 151, 351
Eggleton P. P., 1972, MNRAS, 156, 361
Giddings J. R., 1981, PhD thesis, University of London
Giuricin G., Mardirossian F., 1981, ApJS, 46, 1
Glazunova L. V., Mkrtichian D. E., Rostophchin S. I., 2011, MNRAS, 415, 2238
Hadrava P., 1995, A&AS, 114, 393
Hensberge H., Pavlovski K., Verschueren W., 2000, A&A, 358, 553
Hilditch R. W., 1984, MNRAS, 211, 943
Hilditch R. W., 2001, Close Binary Stars. Cambridge Univ. Press, Cambridge
Hilditch R. W., 2005, Observatory, 125, 72
Hurley J. R., Tout C. A., Pols O. R., 2002, MNRAS, 329, 897
İbanoğlu C., Dervişoğlu A., Çakırlı Ö., Sipahi E., Yüce K., 2012, MNRAS, 419, 1472
Ilijić S., Hensberge H., Pavlovski K., Freyhammer L. S., 2004, in Hilditch R. W., Hensberge H., Pavlovski K., eds, ASP Conf. Ser. Vol. 318, Spectroscopically and Spatially Resolving the Components of the Close Binary Stars. Astron. Soc. Pac., San Francisco, p. 111
Kovachev B. J., Seggewiss W., 1975, A&AS, 19, 395
Napiwotzki R., Schoenberner D., Wenske V., 1993, A&A, 268, 653
Nelson C. A., Eggleton P. P., 2001, ApJ, 552, 664
Nieva M. F., 2013, A&A, 550, A26
Nieva M. F., Przybilla N., 2007, A&A, 467, 295
Nieva M. F., Przybilla N., 2012, A&A, 539, A143
Nieva M. F., Simón-Díaz S., 2011, A&A, 532, A2

Parthasarathy M., Lambert D. L., Tomkin J., 1983, MNRAS, 203, 1063
Pavlovski K., Hensberge H., 2005, A&A, 455, 232
Pavlovski K., Hensberge H., 2010, in Prša A., Zejda M., eds, ASP Conf. Ser. Vol. 435, Binaries - Key to Comprehension of the Universe. Astron. Soc. Pac., San Francisco, p. 207
Pavlovski K., Southworth J., 2009, MNRAS, 455, 232
Pavlovski K., Southworth J., 2012, in Richards M. T., Hubeny I., eds, Proc. IAU Symp. 282, From Interacting Binaries to Exoplanets: Essential Modeling Tools. Cambridge Univ. Press, Cambridge, p. 359
Pfeiffer M. J., Frank C., Baumueller D., Fuhrmann K., Gehren T., 1998, A&AS, 130, 381
Prša A., Zwitter T., 2005, ApJ, 628, 426
Przybilla N., Firnstein M., Nieva M. F., Meynet G., Maeder A., 2010, A&A, 517, A38
Rovithis P., Rovithis-Livaniou H., 1980, Ap&SS, 70, 483

Saad S., Nouh M., 2011, Bull. Astron. Soc. India, 39, 277
Sarna M. J., 1992, MNRAS, 259, 17
Sarna M. J., De Greve J.-P., 1994, A&A, 281, 433
Sarna M. J., De Greve J.-P., 1996, QJRAS, 37, 11
Simon K. P., Sturm E., 1994, A&A, 281, 286
Simón-Díaz S., 2010, A&A, 510, A22
Söderhjelm S., 1978, A&A, 66, 161
Stancliffe R. J., Eldridge J. J., 2009, MNRAS, 396, 1699
Tamajo E., Pavlovski K., Southworth J., 2011, A&A, 526, A76
Tomkin J., Lambert D. L., Lemke M., 1993, MNRAS, 265, 581
van der Veen W. E. C. J., 1984, A&AS, 57, 139
Webbink R. F., 1976, ApJ, 209, 829

This paper has been typeset from a TEX/LATEX file prepared by the author.